Applied Physics Letters

Electromechanical coupling and gigahertz elastic properties of ScAlN films near phase boundary

Cite as: Appl. Phys. Lett. **105**, 122907 (2014); https://doi.org/10.1063/1.4896262
Submitted: 29 July 2014 • Accepted: 03 September 2014 • Published Online: 26 September 2014

Takahiko Yanagitani and Masashi Suzuki

ARTICLES YOU MAY BE INTERESTED IN

AlScN: A III-V semiconductor based ferroelectric
Journal of Applied Physics **125**, 114103 (2019); https://doi.org/10.1063/1.5084945

Elastic constants and critical thicknesses of ScGaN and ScAlN
Journal of Applied Physics **114**, 243516 (2013); https://doi.org/10.1063/1.4848036

Influence of growth temperature and scandium concentration on piezoelectric response of scandium aluminum nitride alloy thin films
Applied Physics Letters **95**, 162107 (2009); https://doi.org/10.1063/1.3251072

Lock-in Amplifiers up to 600 MHz

© 2014 Author(s).

AIP Publishing

APPLIED PHYSICS LETTERS 105, 122907 (2014)

Electromechanical coupling and gigahertz elastic properties of ScAlN films near phase boundary

Takahiko Yanagitani[a] and Masashi Suzuki
Graduate School of Engineering, Nagoya Institute of Technology, Nagoya 466-8555, Japan

(Received 29 July 2014; accepted 3 September 2014; published online 26 September 2014)

The electromechanical coupling, elastic properties, and temperature coefficient of elastic constant c_{33}^{D} of $Sc_xAl_{(1-x)}N$ films with high Sc concentration (x) of 0–0.70 were experimentally investigated. Near the phase boundary, a $Sc_{0.41}Al_{0.59}N$ film exhibited a maximum thickness extensional mode electromechanical coupling coefficient k_t^2 of 12% ($k_t = 0.35$), which is almost double the value of 6.4% for typical pure AlN films. In the region of $0 < x < 0.2$, the electromechanical coupling was confirmed to increase without any detectable deterioration in the temperature stability of c_{33}^{D} ($=-54.5$ ppm/°C). This region is favorable in terms of temperature stability and is suitable for wideband resonator filter applications. © *2014 Author(s). All article content, except where otherwise noted, is licensed under a Creative Commons Attribution 3.0 Unported License*. [http://dx.doi.org/10.1063/1.4896262]

AlN film bulk acoustic wave (BAW) resonator filters are promising for application for mobile communication applications that operate at over 5 GHz.[1,2] The low electromechanical coupling of AlN films which determines the bandwidth of the filter is a drawback, although they do offer Q factor.[3] The large bandwidth of Sc doped AlN resonators has therefore received increasing interest in recent years.[4–6] In 2006, Alsaad and Ahmad predicted the enhancement of piezoelectricity through the Sc doping of GaN in a first principle calculation.[7] After that Akiyama *et al*. experimentally determined a large intrinsic d_{33} piezoelectric constant in Sc doped AlN films[8] and our group reported ScAlN film BAW resonators for the first time.[4] More recently, these studies have been extended to the polarization inverted resonators[9] and YbGaN resonators.[10]

Recent $Sc_xAl_{(1-x)}N$ resonator studies[5,6] have focused on the low Sc concentration region ($x < 0.15$), probably either because the acoustic wave attenuation loss (1/Q factor) in high Sc concentration films was expected to be too large for use as practical resonators or because it is difficult to realize a highly oriented film in the high Sc concentration region, despite the fact that electromechanical coupling has been demonstrated to be proportional to the Sc concentration. However, GHz surface acoustic wave filters with high Q value of 660 were recently reported in a high Sc concentration film on a SiC substrate structure.[11] We can expect that high Q multilayered HBARs (high-overtone bulk acoustic resonators) or surface acoustic wave resonators will be realized even in high Sc concentration films through combinations with high Q materials such as single crystalline diamond substrates. It is important to be able to predict the physical properties near the phase boundary that appear near the high Sc concentration (x) of 0.5.[8,12] Wingqvist *et al.* theoretically predicted the electromechanical coupling of 30%-Sc-concentration ($x < 0.3$) films from the experimental dielectric constant ε_{33}, the theoretical piezoelectric constant e_{33}, and the elastic constant c_{33}.[13]

In this study, the electromechanical coupling, elastic properties, and temperature coefficient of the elastic constant c_{33}^{D} of $Sc_xAl_{(1-x)}N$ films with $x = 0$–0.70 were experimentally investigated. Highly oriented ScAlN films were prepared through Sc ingot sputtering deposition using a single sputtering source.

Single sputtering sources with ScAl alloy metal targets[4,6,14] and dual sputtering sources with Sc and Al metal targets[5,8,11,13] are commonly used for ScAlN growth. These methods, however, are not suitable for preparing samples with different Sc concentrations. High Sc concentration ScAl alloys are difficult to synthesize, and a number of alloy targets for each Sc concentration are required in the experiments. Sc metal targets are easily oxidized in air,[10] and furthermore, pre-sputtering cleaning of the target surface is ineffective for overcoming this problem because the oxygen penetrates beyond the surface of the target. Sc ingot sputtering deposition makes it possible to use fresh and high purity Sc metal for each deposition.

ScAlN films with thicknesses of 4–5 μm were grown on a highly oriented Ti bottom electrode (rocking curve FWHM = 4°) on a silica glass substrate ($25 \times 50 \times 0.5$ mm^3). Sc metal ingots were placed on an Al metal target in a conventional RF magnetron sputtering system. Eleven samples with 0–3.0 g of Sc ingot were prepared at 0.25 g intervals. Two additional samples were also prepared near the phase boundary. The Al metal target was not strongly fixed to the cold cathode, allowing the target temperature to increase. This accelerates the nitridation of the Al target surface during sputtering.

Figure 1(a) shows the Sc concentration of the films determined by an energy dispersive X-ray spectroscopy (EDX), as a function of the weight of Sc introduced. A proportional increase in the Sc concentration with increasing amount of Sc ingot was observed. The X-ray diffraction (XRD) rocking curve FWHM values for the $Sc_xAl_{(1-x)}N$ films are plotted in Fig. 1(b). High and constant crystalline orientations were obtained in the region of $0 < x < 0.4$. The c-axis lengths were determined from the (0002) XRD peak positions. The c-axis lengths as a function of the Sc

[a]Electronic mail: yana@nitech.ac.jp

 © Author(s) 2014

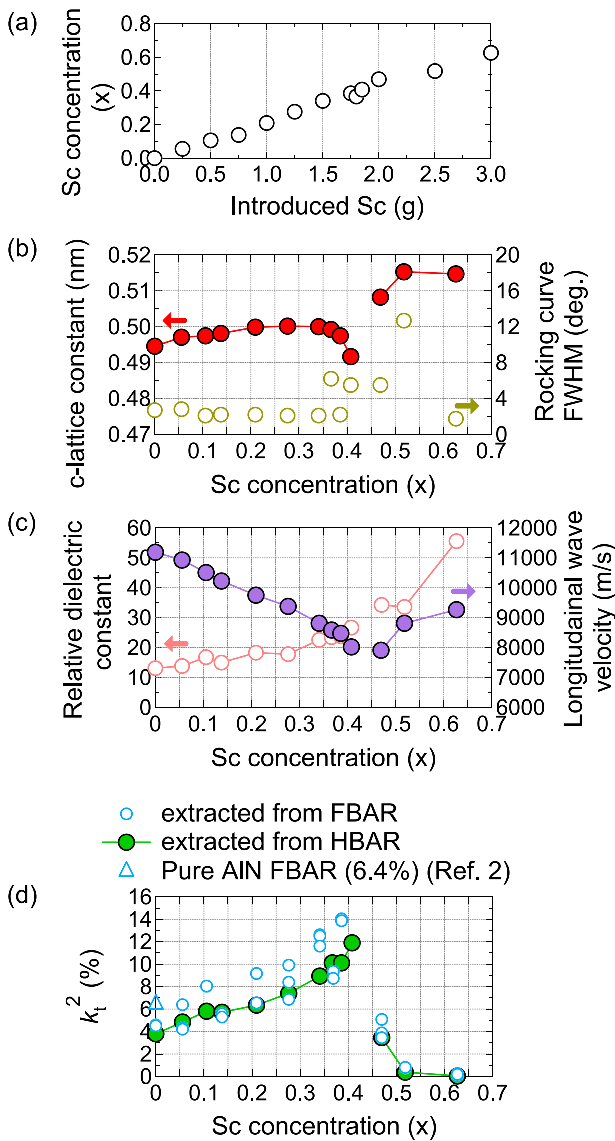

FIG. 1. (a) Sc concentration (x) of the films as a function of the weight of Sc introduced. (b) c-axis lattice lengths (red solid circles) determined from the (0002) XRD peak positions as a function of the Sc concentration. Also plotted are the XRD rocking curve FWHM values (brown open circles). (c) Relative dielectric constant (pink open circles) and longitudinal wave velocity V (purple solid circles) as functions of the Sc concentration. The V and k_t^2 values for the films were determined from the frequency and loss values at minimum point of the experimental conversion loss curves of the $Sc_xAl_{(1-x)}N$ film HBARs, respectively, by comparison with the theoretical curves obtained from a four-layered Mason's equivalent circuit model.[9,15,16] (d) k_t^2 as a function of the Sc concentration. Green solid circles show k_t^2 extracted from the HBARs (including the substrate) and the blue open circles show k_t^2 extracted from the FBARs (free standing membranes).

concentration are also shown in Fig. 1(b). The c-axis length gradually increased as the Sc concentration was increased in the region of $0 < x < 0.3$, but decreased rapidly in the $0.35 < x < 0.4$ region. A discontinuity was observed near $x = 0.43$–0.45. After this point, the c-axis lattice lengths at $x > 0.45$ were found to be larger than those in the region of $0 < x < 0.4$.

Next, HBAR structures consisting of Cu (80–150 nm)/(0001)ScAlN (4–5 μm)/(0001)Ti(90–250 nm)/silica glass substrate (0.5 mm) were prepared in order to extract the relative dielectric constant, the electromechanical coupling coefficient k_t, and the elastic constant c_{33}^E of the films.

The relative dielectric constant of the films was determined from the capacitances (extracted from the slope of admittance vs. frequency), the top electrode areas and the film thicknesses (measured by a stylus profilometer (SE500, Kosaka Laboratory Ltd.)). The relative dielectric constant increased with increasing Sc concentration, as shown in Fig 1(c). This result is in agreement with that reported by Wingqvist *et al.*[13]

The k_t and c_{33}^E of the films were determined by comparing the experimental conversion loss curves of the resonators with theoretical conversion loss curves.[9,15,16] This method makes it possible to determine the physical properties of the piezoelectric layer without the use of a substrate removed structure.[9,15,16] When an electric field is applied to the electrodes, an acoustic wave is generated via a piezoelectric effect and propagates through the substrate. This acoustic wave is reflected at the bottom surface of substrate and returns to the electrodes. These echo signals can be observed electrically again, due to a piezoelectric effect. The losses in this process are known as insertion losses (which are twice the conversion loss) and includes a round-trip of (i) the piezoelectric electro-mechanical conversion loss, (ii) the electric mismatch loss between the capacitive impedance of the film and the 50 Ω measurement system, (iii) the acoustic wave transmission loss at the boundary of each layer and the substrate, and (iv) the acoustic wave propagation and diffraction losses in the substrate.[9,15,16] (ii) and (iii) can be simulated using a Mason's equivalent circuit model including each layer. Therefore, (i) the degree of electro-mechanical conversion k_t can be extracted from the conversion loss.

On the other hand, the minimum points on the conversion loss curve show thickness extensional mode resonance frequencies. The longitudinal wave velocity V ($=\sqrt{c_{33}^D/\rho}$, where c_{33}^D is the piezoelectrically stiffened elastic constant) can be determined from the fundamental mode parallel resonance frequency f_p and the film thickness d by using the relationship $V = 2d\,f_p$, if the mechanical effects of the top and bottom electrodes are ignored. To take account of the effect of the electrodes, accurate k_t^2 and V values for the films were determined from the experimental loss and frequency values at minimum point on the curves, respectively, through comparison with the theoretical curves obtained from a four-layered one dimensional Mason's equivalent circuit model.[9,15,16]

As shown in Fig. 1(c), the longitudinal wave velocity decreased with increasing Sc from x = 0 to 0.41. The velocity of the $Sc_{0.41}Al_{0.59}N$ film near the phase boundary was 8020 m/s, which is 72% of 11132 m/s, the value for an AlN single crystal.[17]

Figure 1(d) shows k_t^2 as function of the Sc concentration. The solid circles show k_t^2 extracted from the HBARs (including a substrate). k_t^2 increased with increasing Sc concentration from x = 0 to 0.41. A significant decrease in k_t^2 was observed for x > 0.47. This decrease may be due to the phase transition from a piezoelectric wurtzite to a non-piezoelectric cubic.[8] The $Sc_{0.41}Al_{0.59}N$ film near the phase boundary exhibited the maximum k_t^2 value of 12% which is 1.9 times higher that for typical pure AlN films sandwiched between heavy Mo electrodes (6.4%).[3] To demonstrate the validity of the k_t^2 measurement from the conversion loss of

the HBAR, k_t^2 estimation through the common resonance-antiresonance method was also carried out using a film bulk acoustic wave resonator (FBAR) structure (without a substrate). Three FBARs for each Sc concentration (36 in total) were prepared from the HBARs (with a substrate). Free-standing FBAR structures were obtained by peeling the membrane part off the substrate using Scotch tape. The k_t^2 value for the FBAR was estimated from the series resonance frequency f_s and the parallel resonance frequency f_p, using the equation $k_t^2 = (\pi/2)\,(f_s/f_p)\,\tan\{(\pi/2)\,[(f_p - f_s)/f_p]\}$. f_s and f_p were determined from the peak frequency of the real part of the admittance and impedance, respectively. The k_t^2 values extracted from the FBARs are also plotted (open circles) in Fig. 1(d). A significant difference in k_t^2 between the FBARs and HBARs was not observed, indicating that the conversion loss method in this study is reasonably valid.

Substituting the V values in Fig. 1(c) and the k_t^2 values (from the HBARs) in Fig. 1(d) into $c_{33}^E = (1 - k_t^2)\,\rho V^2$, we obtain the c_{33}^E as a function of the Sc concentration, assuming that the density ρ of the $Sc_xAl_{(1-x)}N$ film does not vary with x. As shown in Fig. 2, although the resulting c_{33}^E is somewhat higher than the theoretical c_{33}^E values reported by Moram's group,[18] the rate of the decrease of c_{33}^E with x in the present experiment is almost the same as that obtained in the calculation.[18]

The temperature coefficient of the elastic constant c_{33}^D ($= (\partial c_{33}^D/\partial T)/c_{33}^D$) of the piezoelectric layer is an important factor for resonator filter applications because it determines the temperature stability of the filter. The temperature coefficient of frequency (TCF $= (\partial f_p/\partial T)/f_p$) can be written as

$$\frac{1}{f_p}\frac{\partial f_p}{\partial T} = \frac{1}{2}\left(\frac{1}{c_{33}^D}\frac{\partial c_{33}^D}{\partial T} - \frac{1}{\rho}\frac{\partial \rho}{\partial T}\right) - \frac{1}{d}\frac{\partial d}{\partial T} \qquad (1)$$

when the effect of using relatively thin top and bottom electrodes is small. Since the effect of thermal expansion on the resonance frequency is an order of magnitude smaller than that of elastic change, $(\partial c_{33}^D/\partial T)/c_{33}^D$ can be estimated from the TCF if the thermal expansion terms of $(\partial\rho/\partial T)/\rho$ and $(\partial d/\partial T)/d$ are not taken into account. The $(\partial c_{33}^D/\partial T)/c_{33}^D$ values for the ScAlN films were estimated using a linear approximation of the parallel resonance frequencies of the FBARs in the temperature range of 30–90 °C. Figure 3 shows $(\partial c_{33}^D/\partial T)/c_{33}^D$ as function of the Sc concentration. Three $(\partial c_{33}^D/\partial T)/c_{33}^D$ values were extracted from three FBARs for each Sc concentration. The value of $(\partial c_{33}^D/\partial T)/c_{33}^D$ for the ScAlN films decreases with increasing Sc concentration. This decrease may be due to flattening of the potential energy landscape in ScAlN. Tasnadi *et al.* theoretically predicted that ScAlN has a flatter potential energy landscape than AlN.[12] The small curvature of the potential energy landscape indicates elastic softening. $(\partial c_{33}^D/\partial T)/c_{33}^D$ ($=-54.5$ ppm/°C on average) is observed to be almost independent of x in the region of $0 < x < 0.2$, where k_t^2 was confirmed to increase with x. This feature is attractive for resonator filter applications.

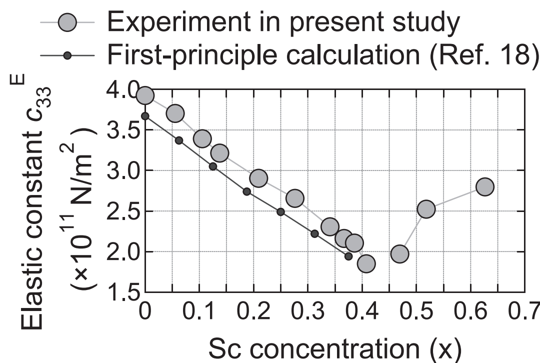

FIG. 2. Elastic constant c_{33}^E as a function of the Sc concentration (x). c_{33}^E was obtained by substituting the values of V in Fig. 1(c) and the k_t^2 values (from the HBARs) in Fig. 1(d) into $c_{33}^E = (1 - k_t^2)\,\rho V^2$. The density ρ of the $Sc_xAl_{(1-x)}N$ film is assumed not to vary with x. The theoretically predicted values for c_{33}^E reported by Moram's group[18] are also plotted.

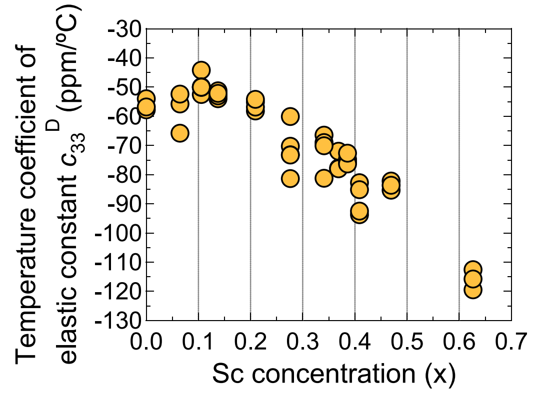

FIG. 3. $(\partial c_{33}^D/\partial T)/c_{33}^D$ estimated from the TCF as a function of the Sc concentration (x). The thermal expansion terms of $(\partial\rho/\partial T)/\rho$ and $(\partial d/\partial T)/d$ are not taken into account in the estimation. The values of $(\partial c_{33}^D/\partial T)/c_{33}^D$ were determined using a linear approximation of the parallel resonance frequencies of the FBARs in the temperature range of 30–90 °C. Three $(\partial c_{33}^D/\partial T)/c_{33}^D$ values were extracted from three FBARs for each Sc concentration.

In conclusion, we experimentally investigated the electromechanical coupling, elastic properties, and temperature coefficient of the elastic constant c_{33}^D of $Sc_xAl_{(1-x)}N$ films with Sc concentrations in the region of $0 < x < 0.70$. The maximum k_t^2 value of 12% ($k_t = 0.35$), which is 1.9 times that of typical pure AlN films (6.4%), was found at $x = 0.41$ near the phase boundary. A stable TCF ($=-27.2$ ppm/°C) with a definite increase in electromechanical coupling in the $0 < x < 0.2$ region is favorable for resonator filter applications. The enhancement of piezoelectricity at the phase boundary of ScAlN, which is the largest electromechanical coupling in paraelectric materials, is interesting from the viewpoint of condensed matter physics. The dielectric constant, which is far smaller than that of ferroelectric materials, is attractive for applications to large aperture GHz ultrasonic transducers and energy harvesters.

[1]R. Lanz and P. Muralt, IEEE Trans. Ultrason. Ferroelectr. Freq. Control **52**, 936 (2005).
[2]M. Hara, T. Yokoyama, T. Sakashita, S. Taniguchi, M. Iwaki, T. Nishihara, M. Ueda, and Y. Satoh, Jpn. J. Appl. Phys., Part 1 **49**, 07HD13 (2010).
[3]T. Nishihara, T. Yokoyama, T. Miyashita, and Y. Satoh, in *Proc. IEEE Ultrason. Symp.* (IEEE, 2002), p. 969.
[4]T. Yanagitani, K. Arakawa, K. Kano, A. Teshigahara, and M. Akiyama, in *Proc. IEEE Ultrason. Symp.* (IEEE, 2010), p. 2095.
[5]M. Moreira, J. Bjurstrom, I. Katardjev, and V. Yantchev, Vacuum **86**, 23 (2011).

[6]R. Matloub, A. Artieda, C. Sandu, E. Milyutin, and P. Muralt, Appl. Phys. Lett. **99**, 092903 (2011).
[7]A. Alsaad and A. Ahmad, Eur. Phys. J. B **54**, 151 (2006).
[8]M. Akiyama, T. Kamohara, K. Kano, A. Teshigahara, Y. Takeuchi, and N. Kawahara, Adv. Mater. **21**, 593 (2008).
[9]T. Yanagitani and M. Suzuki, Appl. Phys. Lett. **104**, 082911 (2014).
[10]M. Suzuki, T. Yanagitani, and H. Odagawa, Appl. Phys. Lett. **104**, 172905 (2014).
[11]K. Hashimoto, S. Sato, A. Teshigahara, T. Nakahara, and K. Kano, IEEE Trans. Ultrason. Ferroelectr. Freq. Control **60**, 637 (2013).
[12]F. Tasnadi, B. Alling, C. Hoglund, G. Wingqvist, J. Brich, L. Hultman, and I. A. Abrikosov, Phys. Rev. Lett. **104**, 137601 (2010).
[13]G. Wingqvist, F. Tasnadi, A. Zukauskaite, J. Birch, H. Arwin, and L. Hultman, Appl. Phys. Lett. **97**, 112902 (2010).
[14]S. Fujii, S. Shimizu, M. Sumisaka, Y. Suzuki, S. Otomo, T. Omori, and K-Y. Hashimoto, *Proc. IEEE Freq. Control Symp.* (IEEE, 2014), p. 350.
[15]J. D. Larson, D. K. Winslow, and L. T. Zitelli, IEEE Trans. Sonics Ultrason. **19**, 18 (1972).
[16]T. Yanagitani and M. Kiuchi, J. Appl. Phys. **102**, 044115 (2007).
[17]Y. Ohashi, M. Arakawa, J. Kushibiki, B. M. Epelbaum, and A. Winnacker, Appl. Phys. Express **1**, 077004 (2008).
[18]S. Zhang, W. Y. Fu, D. Holec, C. J. Humphreys, and M. A. Moram, J. Appl. Phys. **114**, 243516 (2013).